# Exposure of Remote Organs and Associated Cancer Risks from Tangential and Multi-Field Breast Cancer Radiotherapy

C. Simonetto, H. Rennau, J. Remmele, S. Sebb, P. Kundrát, M. Eidemüller, U. Wolf, G. Hildebrandt

Corresponding author: Cristoforo Simonetto, cristoforo.simonetto@helmholtz-muenchen.de, Institute of Radiation Protection, Helmholtz Zentrum München Deutsches Forschungszentrum für Gesundheit und Umwelt (GmbH), Ingolstädter Landstraße 1, 85764 Neuherberg, Germany;

Hannes Rennau, hannes.rennau@uni-rostock.de, Universitätsmedizin Rostock Klinik und Poliklinik für Strahlentherapie, MVZ der Universitätsmedizin Rostock am Standort Südstadt gGmbH, Südring 75, 18059 Rostock, Germany

Julia Remmele, julia.remmele@medizin.uni-leipzig.de, Universität Leipzig Klinik für Strahlentherapie, Stephanstraße 9a, 04103 Leipzig, Germany

Sabine Sebb, sabine.sebb@med.uni-rostock.de, Universitätsmedizin Rostock Klinik und Poliklinik für Strahlentherapie, MVZ der Universitätsmedizin Rostock am Standort Südstadt gGmbH, Südring 75, 18059 Rostock, Germany

Pavel Kundrát, pavel.kundrat@helmholtz-muenchen.de, Institute of Radiation Protection, Helmholtz Zentrum München Deutsches Forschungszentrum für Gesundheit und Umwelt (GmbH), Ingolstädter Landstraße 1, 85764 Neuherberg, Germany

Markus Eidemüller, markus.eidemueller@helmholtz-muenchen.de, Institute of Radiation Protection, Helmholtz Zentrum München Deutsches Forschungszentrum für Gesundheit und Umwelt (GmbH), Ingolstädter Landstraße 1, 85764 Neuherberg, Germany

Ulrich Wolf, ulrich.wolf@medizin.uni-leipzig.de, Universität Leipzig Klinik für Strahlentherapie, Stephanstraße 9a, 04103 Leipzig, Germany

Guido Hildebrandt, guido.hildebrandt@uni-rostock.de, Universitätsmedizin Rostock Klinik und Poliklinik für Strahlentherapie, MVZ der Universitätsmedizin Rostock am Standort Südstadt gGmbH, Südring 75, 18059 Rostock, Germany

## Ethical Standards

The study was approved by the ethics committee of the University Medicine Rostock (A 2014-0128).

## Acknowledgements

This work was supported by the German Federal Ministry of Education and Research (BMBF) under contract number 02NUK026 (PASSOS).

The final publication is available at link.springer.com, Strahlenther. Onkol. 195, 32-42 (2018).

# Exposure of Remote Organs and Associated Cancer Risks from Tangential and Multi-Field Breast Cancer Radiotherapy

**Purpose:** With increasing cure rates of breast cancer, radiotherapy-induced cancers have become an important issue. This study aims at estimating secondary cancer risks for different treatment techniques, taking into account organs throughout the body.

**Material and Methods:** Organ doses were evaluated for a tangential three-dimensional conformal (3D-CRT) and a multi-field intensity-modulated radiotherapy (IMRT) plan using a validated, Monte Carlo based, treatment planning system. Effects of wedges and of forward versus inverse planning were systematically investigated on the basis of phantom measurements. Organ-specific cancer risks were estimated using risk coefficients derived from radiotherapy patients or from the atomic bomb survivors.

**Results:** In the 3D-CRT plan mean organ doses could be kept below 1 Gy for more remote organs than lung, heart, and contralateral breast, and declined to a few cGy for organs in the lower torso. Multi-field IMRT led to considerably higher mean doses in organs at risk, the difference being higher than 50% for many organs. Likewise, peripheral radiation burden was increased by external wedges. No difference was observed for forward versus inverse planning. Despite the lower doses, the total estimated secondary cancer risk in more remote organs was comparable to that in the lung or the contralateral breast. For multi-field IMRT it was 75% higher than for 3D-CRT without external wedges.

**Conclusion:** Remote organs are important for assessment of radiation-induced cancer risk. Remote doses can be reduced effectively by application of a tangential field configuration and a linear accelerator set-up with low head scatter radiation.

Keywords: radiotherapy, breast cancer, secondary cancer, peripheral dose, IMRT, 3D-CRT

## Dosen und Zweittumor-Risiken in entfernt liegenden Organen bei tangentialer und bei Vielfeld-Strahlentherapie der Brust

**Ziel:** Wegen steigender Heilungsraten von Brustkrebs gewinnt das Risiko durch die Strahlentherapie Zweittumore zu verursachen an Bedeutung. Ziel dieser Studie war es, die Zweittumor-Risiken für verschiedene Behandlungstechniken abzuschätzen und dabei auch die Organe zu berücksichtigen, die sich weiter entfernt vom Feld befinden.

**Material und Methoden:** Mit einem validierten Bestrahlungsplanungssystem mit Monte Carlo Algorithmus wurden Organdosen berechnet für tangentiale, dreidimensionale konformale Strahlentherapie (3D-CRT) und für intensitätsmodulierte Strahlentherapie (IMRT) mit Feldern aus vielen Richtungen. Mit Phantom-Messungen wurden systematisch die Verwendung von Keilfiltern und der Einfluss von inverser Planung untersucht. Zur Berechnung von Krebsrisiken wurden sowohl Risikokoeffizienten aus Studien zu Strahlentherapie-Patienten als auch zu Atombomben-Überlebenden verwendet.

**Ergebnisse:** Im 3D-CRT-Plan waren die mittleren Organdosen für weiter entfernte Organe als Lunge, Herz und kontralaterale Brust unterhalb von 1 Gy und fielen mit der Entfernung im Torso bis auf einige cGy ab. Die IMRT-Technik mit vielen Feldern führte zu deutlich höheren mittleren Dosen in allen Organen außerhalb des Zielvolumens – für viele Organe um mehr als 50%. Ebenso erhöhten externe Keilfilter die Strahlenbelastung in entfernten Organen. Kein Unterschied konnte allerdings zwischen inverser und Vorwärts-Planung festgestellt werden.

Trotz der geringeren Dosen trugen in Summe weiter entfernte Organe ähnlich hoch zum Zweittumor-Risiko bei wie die Lunge oder die kontralaterale Brust. Für die IMRT-Technik war dieser Beitrag um 75% höher als für 3D-CRT ohne externe Keilfilter.

**Schlussfolgerung**: Bei der Abschätzung von Zweittumor-Risiken sind auch entferntere Organe als Lunge und kontralaterale Brust wichtig. Deren Exposition kann durch eine tangentiale Feldkonfiguration und mit einem Beschleuniger-Aufbau mit geringer Streustrahlung effektiv reduziert werden.

## Introduction

Breast cancer (BC) is the most common cancer in women with an age-standardized incidence rate of about 90 per 100,000 women in Western Europe [1]. In the last decades, the life expectancy of BC patients increased substantially due to screening-related earlier detection and advances in treatment. The 5-year net survival is already above 85% in many countries [2]. Radiotherapy is part of the standard treatment after breast conserving surgery for invasive tumours [3], and possible late side effects are thus of increasing relevance. While studies on breast cancer patients have shown that radiotherapy elevates the risks for cancers in organs close to the irradiation fields and for cardiac diseases [3,4], still important open questions relate to the effect of contemporary radiotherapy techniques on cardiac diseases, to individual differences in risks, and to the impact of out-of-field exposure on secondary cancer risk. The German PASSOS project [5] addressed all of these issues, and some results on heart exposure and cardiac risk can be found in refs. [6-9]. The present manuscript focuses on the assessment of doses and cancer risks in organs more remote to the treated breast than lung, heart or contralateral breast. Possible cancer risks in these more remote organs have become increasingly important in the last years as the improvement of target coverage and the reduction of the high dose volumes that can be achieved with modern multi-field techniques is always at the cost of a higher "low-dose bath".

Doses to some remote organs for different radiation techniques in BC radiotherapy have been published by several authors [10-14]. However, dose estimates differ greatly between publications. Only in one publication [11] an exhaustive number of organs was considered. Additionally, there is a huge spread in risk estimates [15] due to the application of various risk models, of which many were compiled for general radiation protection purposes and not for breast cancer patients. Therefore, the aim of the present study is to complement and extend previous studies on remote organ doses and to provide realistic estimates of the radiation-induced cancer risks.

## Materials and Methods

To achieve these aims, we proceeded in several steps, described in detail below. First, we estimated organ doses for a tangential 3D-CRT and a multi-field IMRT technique with a Monte Carlo based treatment planning system. Second, based on these doses, radiation-induced cancer risks were calculated. Calculations employ dose-response studies of BC radiotherapy for organs close to the fields, i.e. lung, contralateral breast and oesophagus. For more remote organs, for which the low doses and associated effects hinder dose-response studies in BC patients, we applied results from the atomic bomb survivors of Hiroshima and Nagasaki. Finally, the variability in doses from different tangential techniques and in different individuals was investigated.

### *Organ dose assessment*

Tangential and multi-field techniques lead to rather different dose distributions in the body. These differences were investigated by treatment plan calculations of a field-in-field 3D-CRT and a step-and-shoot multi-field IMRT plan. Both techniques were planned with flattening

filters and without wedges, using 6 MV photon beams. The prescribed dose to the whole breast was 50.4 Gy plus an additional boost of 16 Gy to the tumour bed. Objectives were minimization of the exposures of contralateral breast, ipsilateral lung and heart while keeping the dose within the planning target volume (PTV) between 95% and 107% of the prescribed dose. For small volumes within the PTV, maximum doses of up to 110% of the prescribed dose were accepted. The treatment fields for multi-field IMRT were based on the field direction of the respective 3D-CRT plan, with 4 different fields from each tangential direction (separated each by 10 degrees). Additional four to eight fields were added, each separated by 40 degrees, omitting fields that comprise the contralateral mammilla or that irradiate the contralateral lung before reaching the PTV. The resulting dose distributions are depicted in Figures S1 and S2 in the supplementary material.

Breast-cancer radiotherapy is usually planned based on a Computed Tomography (CT) scan of the patient's thorax. To calculate the exposure for more remote organs, it was necessary to create the plans on a 'whole-body' CT scan that was obtained in connection with positron emission tomography from a female patient with cancer in the left lung. During CT, the patient was in supine position, similar to BC radiotherapy, see Fig. S3 in the supplementary material. With a height of 163 cm the patient was nearly European average [16] and had a normal weight of 55 kg. The whole-body CT covered a cranio-caudal distance of about 103 cm and thus included the entire torso and head, the upper arms, and parts of the thighs. The contouring of the organs was conducted by a medical physicist and a medical doctor without using any auto-contouring features within the treatment planning system. To investigate the dosimetric differences between treatments of left- and right-sided breast tumours, treatment plans for both sides were created with similar gantry angles for both whole-breast and boost-volume on each side. For the planning, IPLAN 4.5.4 was applied, commissioned for a Vero accelerator (BrainLAB AG, Feldkirchen, Germany). IPLAN uses Pencil Beam for the optimization process and the Voxel-Monte-Carlo-Algorithm [17] for the final dose calculation. The Monte Carlo calculation is based on the analytical energy profile of the accelerator head modified by the multi-leaf collimator shaping the individual photon beam, which allows for a fast dose calculation [18,19]. The accuracy of the dose calculation was validated by phantom measurements with a single 10×10 $cm^2$ open field and showed consistency within about 30% even for distances up to 40 cm from the irradiated area, see Figures S4, S5 and S6 in the supplementary material.

***Estimating cancer risks***

Cancer risks were derived by applying published, organ-specific risk models. For the organs not delineated in the CT, mean doses have been estimated from the dose-volume histograms of nearby organs. This is a rather crude approach, but acceptable in view of the large dose uncertainty and variability. Details can be found in Table S1 in the supplementary material.

Studies on the cancer risk in the lung [20], contralateral breast [21] and oesophagus [22] after BC radiotherapy were applied in this work. The respective publications are tabulated together with best estimates of risk coefficients in Table S2 in the supplementary material. Here we treat odds ratios as equivalent to relative risks since the investigated diseases are rare. Risk coefficients for other solid cancer sites were based on a study of atomic bomb survivors [23], evaluated for an age at exposure of 50 years and an attained age of 70 years, tabulated in Table S3 in the supplementary material. To calculate average relative risks for

several cancer endpoints combined, the radiation-induced relative risk of each organ was weighted by its incidence rate in the German female population aged 50 years and above [24], listed in Table S1 in the supplementary material. These incidence rates were chosen for their completeness including also rare cancer sites. European rates [25] are similar.

The above-mentioned studies assumed the linear no-threshold (LNT) model:

$$RR = 1 + ERR_{pd}\,\overline{D} \tag{1}$$

Here *RR* denotes the relative risk compared to an unexposed person, and the excess relative risk is given by the product of $ERR_{pd}$, the excess relative risk per unit dose, and $\overline{D}$, the mean organ dose. We adopted this model for all solid cancer sites. Leukaemia risk, however, deserves a special treatment as there is evidence for a strong non-linear dose dependence [26,27]. In this case, knowledge of the dose-volume histogram of the active bone marrow is necessary to derive risks. The skeleton was thus contoured in the whole-body CT, and sectioned in 8 different compartments. Dose-volume histograms of each compartment were combined weighted by their active bone marrow content [28], cf. Table S4 in the supplementary material. To infer the risks, a model linear at low doses and exponentially suppressed at high doses was preferred in a study of patients treated for cervical cancer [26]:

$$RR = \frac{1}{V}\int (1 + 0.88\,D)e^{-0.079\,D}dV \tag{2}$$

Here *D* is the local dose in Gy and the integration is performed over the volume of the active bone marrow. For this dose-response relationship, the effect of radiation is maximal at about 10 Gy and decreases for higher doses. On the other hand, the leukaemia risk was observed to be compatible with the LNT in a study of patients with cancer of the uterine corpus [27] with $ERR_{pd}$= 0.13 (95% CI: 0.04; 0.27) per Gy – at least when considering external beam therapy only. Therefore, we will present risk estimates for both models.

Similar to leukaemia, risks for soft-tissue, bone and skin cancers may be affected by high therapeutic as well as by lower doses. However, these risks are not discussed in this work, in particular due to the associated large uncertainties in risk estimates.

In general, calculation of absolute risks depends on age, relative survival, and frequency of the outcome in the studied patient group. A rough estimate, however, is possible by multiplying excess relative risks with general population incidence rates (estimated absolute risk = excess relative risk × incidence rate) where the incidence rates can be found in Table S1 in the supplementary material.

***Different tangential techniques and inter-individual dose variability***

In order to compare different tangential techniques, measurements were performed in an Alderson phantom with thermoluminescence detectors (Type 100-H, rods 1x6mm), inserted at several positions in the trunk and the head of the phantom. With this approach, organ dose distributions cannot be calculated, but it is a reliable method to assess differences between dose distributions of similar shapes.

The following techniques were investigated: first, the same field-in-field 3D-CRT without wedge compensation as studied with Monte Carlo calculations, second, the same technique but using external wedges, and third, a combination of manual and inverse planning was investigated, called 'hybrid IMRT' in the following. The hybrid IMRT was set up as a tangential technique where the main dose contribution (70% to 80%) is delivered by two open fields but dose homogeneity in the PTV is achieved by a number of segmented, inversely planned fields. All techniques were planned with the same main field angles. Plans were generated with Oncentra Masterplan 4.3, commissioned for the Siemens Primus (6MV photon beams).

Finally, in order to obtain information on individual dose variation and the representativeness of our results, doses to some organs in relative vicinity to the treated breast were compared to the PASSOS planning study. Details can be found at the end of the supplementary material. An overview of the different dosimetric approaches in this study is provided in Table 1.

## Results

### *Organ doses in 3D-CRT without wedges and multi-field IMRT*

Mean organ doses calculated by the Monte Carlo based treatment planning system for the whole-body CT are depicted with black, solid symbols in Fig. 1. The multi-field IMRT plan led to higher mean doses in all organs. For the ipsilateral lung, mean doses were 10 Gy for IMRT and 8 Gy for 3D-CRT. For the contralateral breast the IMRT plan resulted in a rather high mean dose of 6 Gy. The other organs shown in Fig. 1 were exposed to less than about 1 Gy with a minimum of roughly 30 mGy. A comparison of our dose estimates to other results from the literature will be drawn in the Discussion section. Numeric dose values, including additional organs and the contribution of the boost, can be found in Table S5 the supplementary material.

For leukaemia, we apply a non-linear risk model. Therefore, a dose-volume histogram for the active bone marrow was derived, and is shown in Fig. 2. As IMRT conforms more precisely to the PTV, the IMRT technique reduced the fraction of bone marrow with very high dose exposure. This reduction, however, applies only to a small volume (less than 1%) and is at the cost of higher doses to the major part of the bone marrow.

### *Cancer risks*

Relative risks of secondary cancer, estimated for the whole-body CT from Monte Carlo calculations are shown in the upper part of Table 2. For 3D-CRT, the relative risk was highest for lung cancer, with a value of about 1.4. For the IMRT plan, the relative risk was even higher for the contralateral breast, due to the much higher dose compared to the 3D-CRT plan, see Fig. 1. For both plans, the non-linear leukaemia model yielded a higher risk than the linear model but the two results were consistent within 90% confidence intervals. Most organs were aggregated (column "other") and their average estimated relative risk, weighted by the cancer

incidence rates, was below 1.1. The aggregation was performed because single-organ risk uncertainties are large in particular for low doses, see the Discussion section. Nevertheless, it might be interesting to state some additional risk estimates in order to understand the contribution of different organs: For right-sided therapy, quite high relative risks of 1.2 for 3D-CRT without wedges and 1.4 for multi-field IMRT were derived for the liver. However, as liver cancer is comparatively rare, the absolute contribution of liver cancer to the total risk is modest. Relatively frequent are cancers of the uterus and the colon. While the dose to the uterus was almost negligible in this study, inference on the colon dose yielded relative risks of 1.06 for the 3D-CRT and 1.1 for the IMRT plan. Similar relative risks were estimated for stomach and pancreas.

Apart from leukaemia, all risk models applied in this study are linear in dose. Therefore, the higher mean doses from the IMRT technique led to higher risks compared to the 3D-CRT technique. According to the linear-exponential dose-response relationship for leukaemia risk, doses around 10 Gy are most detrimental. Compared to 3D-CRT, a larger fraction of active bone marrow was exposed to doses in this range for the IMRT plan (Fig. 2, associated with a higher predicted risk, see Table 2.

Fig. 3 shows absolute risks based on the relative risks from Table 2. The best estimate for the number of radiation-induced cancers in remote organs was close to the number of radiation-induced lung cancer cases, in particular for IMRT. The number of excess cancers in remote organs may also be comparable to the number of excess contralateral breast cancers, which was however highly uncertain.

***Comparing different tangential techniques***

In order to evaluate the impact of variations in the 3D-CRT technique, a direct comparison of doses from different tangential techniques was obtained by thermoluminescence measurements in a phantom. Markers in Fig. 4 show the measured doses at various positions in the phantom including positions in the lung and the heart but also more remote ones such as the head and the abdomen. For each position, doses from the field-in-field 3D-CRT without wedges are plotted in x-direction and doses from other techniques are plotted in the y-direction.

The application of wedges increased the doses. The relative difference was highest for the lowest doses. For example, the dose as obtained from 3D-CRT with wedges was almost 0.5 Gy at a position where it was only 0.2 Gy when applying 3D-CRT without wedges. On the other hand, applying inverse planning with the same main tangents as in the 3D-CRT plan ('Hybrid IMRT') led to doses which were practically indistinguishable from the manual planning.

In order to check independence of these results from the specific plan and anatomy used, we also show as lines data from the PASSOS patient planning study (see supplementary material). They refer to the group average of the dose-volume histograms of the parts of the patients' bodies covered by the planning CTs. The dose of each percentile of the dose-volume histogram for a given treatment technique is plotted against the same percentile for 3D-CRT without wedges. These data are imprecise at low doses (see the Discussion section), but nevertheless do support the findings from the phantom measurements very well.

## Discussion

### *Comparing the doses to the literature*

Several publications have derived dose estimates for some organs for similar treatment techniques. Joosten et al. [11] performed an extensive Monte Carlo study evaluating, amongst others, a wedged 3D-CRT technique and a hybrid IMRT. The hybrid IMRT plan was based on the same tangent fields as the 3D-CRT technique but instead of wedges, two additional intensity modulated tangent fields were applied. Donovan et al. [10], Lee et al. [12] and Han et al. [13] determined the doses to some remote organs by measurements in a phantom. A field-in-field technique was used in Lee et al. and Han et al. without physical wedges. Results of these studies are shown in Fig. 1. Because in Han et al. the field-in-field technique led to practically identical organ doses as an approach with enhanced dynamic wedges, we show only the former. Instead of mean organ doses, organ equivalent doses are presented by Han et al. Organ equivalent doses [29] (not to be confused with the radiation protection concept of equivalent dose) correspond to a weighted dose metric with a relatively small contribution of high doses. They coincide with mean organ doses only in the limit of small doses. For example, the organ equivalent dose to the liver as deduced from our IMRT data for right-sided radiotherapy reads 0.4 Gy to be compared to the mean liver dose of 1.2 Gy. For left-sided radiotherapy it reads 0.3 Gy which is already closer to the mean dose of 0.5 Gy. Therefore, we do not present the data of Han et al. for organs close to the treated breast.

In general, our results agree with those from Joosten et al. and Han et al. The largest relative discrepancy was observed for the liver. However, such two-fold differences can easily originate from inter-individual variation as can be seen for other organs from Fig. S7 in the supplementary material. Our results agree with Han et al. and with Lee et al. in that multi-field IMRT yields higher mean organ doses compared to 3D-CRT without external wedges. On the contrary, Joosten et al. observed lower doses for an IMRT technique compared to a wedged 3D-CRT. Underlying reasons are obvious: First, wedges introduce additional scatter radiation, see Fig. 4. Second, Joosten et al. investigated a hybrid IMRT. As illustrated in Fig. 4, the choice for forward or inverse planning of sub-fields has practically no impact on remote doses as long as the dose is delivered by tangential fields. Therefore, doses from hybrid IMRT rather resemble doses from 3D-CRT without wedges.

On the other hand, Donovan et al. and Lee and al. provide mean doses to the ipsilateral lung which are exceedingly low. Both studies are based on thermoluminescence measurements in a phantom and thus cannot fully capture the dose gradient in the ipsilateral lung even with several detectors. In the study of Lee et al., the beams were directed through the phantom's breast without even touching the lung, see Fig. 2 therein. This was not feasible in any patient in the PASSOS planning study. In Donovan et al. a relatively low prescribed dose of 40 Gy was applied to the whole breast, contrary to 50.4 Gy in the present study that additionally involves boost irradiation. This difference, however, does not suffice to explain the low lung dose. Lung doses after different modern techniques of breast cancer radiotherapy were extensively reviewed in [4,30]. Results from Donovan et al. and Lee et al. are about an order of magnitude below mean ipsilateral lung doses typical for modern radiotherapy [4], plotted as grey rectangles in Fig. 1. Ipsilateral lung doses below 1 Gy were observed only for partial breast irradiation [30]. On the contrary, our results for ipsilateral lung doses are well within the typical range. For the contralateral lung our estimates as well as the difference

between tangential and IMRT technique are somewhat below values regarded as typical in the reviews [4,30].

***Comparing the estimated to observed relative risks***

Many approaches to estimate secondary cancer risks after radiotherapy have been applied in the literature, and the results differ widely [15]. Therefore, it is important to check that results are consistent with the observed excess cases in large patient populations. Meta-analyses of various randomized trials on radiotherapy within the Early Breast Cancer Trialists' Collaborative Group comprise more than 30,000 patients [3]. Organ doses were not available in the meta-analysis. However, relative risks of radiotherapy versus no radiotherapy were derived and are largely consistent with our estimates, see Table 2. Finally, it should be noted that the meta-analysis includes trials with outdated radiotherapy techniques that involve higher doses to organs at risk compared to contemporary techniques. Higher doses may have resulted from extended target volumes, or from older irradiation facilities. Moreover, application of wedges leads to higher exposure far from the main fields, see Fig. 4. Indeed, our estimates for 3D-CRT without wedges tend to be below estimates from the meta-analysis.

***Limitations***

Uncertainties are substantial with regards to many results in the present manuscript. To reduce uncertainty in the dose calculations, we applied a Monte Carlo based algorithm. This algorithm proved to be accurate within about 30% even far from the field, at least when irradiating with a 10×10 cm² open field. Furthermore, individual anatomy is an important factor. Individual organ doses can deviate from the median of a patient cohort by more than a factor of two in both directions, see Fig. S7 in the supplementary material. Moreover, there is variation due to different linac geometries [31], and there is variation related to the individual creation of the treatment plans. Nevertheless, dose estimates for remote organs roughly agree with other studies, see Fig. 1 and respective explanations in the above discussion.

For estimation of the risk of second primary cancers, two additional major sources of uncertainty are involved. First, statistical uncertainty limits the precision of parameters in the risk models. Second, it is unclear how the risks compare between different cohorts and exposure scenarios. For the lung, breast and oesophagus, risk estimates exist from both BC patients and atomic bomb survivors, and although statistical uncertainty is large especially for the BC patients, it is apparent that breast cancer patients show considerably lower risks per unit dose [20-23,32]. A possible explanation is the strong dose inhomogeneity in breast cancer therapy [33]. Dose gradients in remote organs are less strong and mean organ doses are close to or below the mean body dose. In this case, cancer risks derived from the uniform exposure in atomic bomb survivors may be adopted to calculate risks in remote organs in BC radiotherapy. To cover both, atomic bomb survivor and, for higher doses, therapeutic risk data, non-linear models have been proposed [34,35,29]. These models assume that risk coefficients derived from the atomic bomb survivors can be applied to the low-dose regime and a flattening of risk for high doses is imposed in order to be compatible with the results from radiotherapy studies. However, so far no single epidemiological study could provide evidence in favour of a flattening or downturn of lung or breast cancer risk for high doses [36]. To mitigate this problem, we applied risk coefficients derived in studies on BC patients for

some organs close to the treated breast. Even though radiotherapy has evolved during the last decades, these studies yield the best approximation of the dose distribution in the body in contemporary breast cancer radiotherapy, and dependence of risk estimates on possible non-linearity of the dose-response relationship is thus alleviated. A comparison of linear and non-linear risk models for lung cancer risk was carried out in ref. [37] and the non-linear models turned out to overestimate absolute risks. Finally, it should be noted that a flattening or downturn of the dose response for high doses would strengthen the relative importance of the low-dose region. On the other hand, applying results from diverse studies, there may be some variation in risk estimates due to different study designs and populations.

***On the impact of the cancer risk in remote organs***

While relative risks are preferable to compare different studies, absolute risk estimates are more instructive to rate the impact. Rough estimates of absolute risks were derived in Fig. 3 by multiplication of relative risks with general population incidence data. For this approach to be valid it is important to note that the risk for cancer in organs other than breast is similar in breast cancer patients not treated with radiotherapy and the general population [38]. Regarding the risk of contralateral breast cancer, breast cancer patients were under increased risk in the past but introduction of tamoxifen has about halved the number of contralateral breast cancers, being now close to or even below the population average [39,40].

In the meta-analysis of randomized trials [3], an estimated number of 39 radiation-induced cancers in remote organs occurred during about 130,000 years of follow-up. Although associated with large uncertainties, this number is highly compatible with our rough estimate, see Fig. 3. Consistent with our estimates in Fig. 3, a similar number of lung cancers (49) was attributed to radiotherapy in the meta-analysis, and only 15 cases of leukaemia. In view of the strong association of lung cancer risk with smoking behaviour [37,4] the agreement is even better than expected. About 114 cases of contralateral breast cancer were attributed to radiotherapy. However, in most studies included in the meta-analysis, tamoxifen was not administered to the patients. Therefore, for contemporary treatment schemes, radiation-induced risk for contralateral breast cancer may be of very similar magnitude compared to the radiation-induced risk in more remote organs.

Although the above-mentioned radiation-induced risks are not very large, they give a sizeable contribution to the risk-benefit ratio of radiotherapy: For women with a 5-year local recurrence risk above 10%, adjuvant radiotherapy lowers the risk of breast cancer death by 5% during 15 years after treatment [3]. On the other hand, our estimates imply a risk for radiation-induced incidence of cancer of the lung, contralateral breast, remote organs, and leukaemia for 3D-CRT (IMRT) of about 80 (180) cases in 100,000 years (see Fig. 3), which means about 1.2% (2.7%) within 15 years.

**Conclusion**

While the risk of radiation-induced cancer was estimated directly from studies of breast cancer therapy for organs in relative vicinity to the treated breast this was not possible for remote organs. Applying risk coefficients derived from the atomic bomb survivors for other organs, the

estimated absolute number of radiation-induced cancers in more remote organs was of comparable magnitude as the estimated number of radiation-induced lung or contralateral breast cancers. A reduction of peripheral exposure could be achieved by tangential irradiation without external wedges. The same method led also to the lowest exposure of organs close to the treated breast such as the lungs or contralateral breast, and is thus preferable regarding radiation-induced cancer risk.

**References**


1. WHO Breast cancer: prevention and control. http://www.who.int/cancer/detection/breastcancer/en/index1.html. Accessed 9 July 2018
2. Allemani C, Weir HK, Carreira H, Harewood R, Spika D, Wang XS, Bannon F, Ahn JV, Johnson CJ, Bonaventure A, Marcos-Gragera R, Stiller C, Azevedo e Silva G, Chen WQ, Ogunbiyi OJ, Rachet B, Soeberg MJ, You H, Matsuda T, Bielska-Lasota M, Storm H, Tucker TC, Coleman MP, Concord Working Group (2015) Global surveillance of cancer survival 1995-2009: analysis of individual data for 25,676,887 patients from 279 population-based registries in 67 countries (CONCORD-2). Lancet 385 (9972):977-1010. doi:10.1016/S0140-6736(14)62038-9
3. Clarke M, Collins R, Darby S, Davies C, Elphinstone P, Evans V, Godwin J, Gray R, Hicks C, James S, MacKinnon E, McGale P, McHugh T, Peto R, Taylor C, Wang Y, Early Breast Cancer Trialists' Collaborative Group (2005) Effects of radiotherapy and of differences in the extent of surgery for early breast cancer on local recurrence and 15-year survival: an overview of the randomised trials. Lancet 366 (9503):2087-2106. doi:10.1016/S0140-6736(05)67887-7
4. Taylor C, Correa C, Duane FK, Aznar MC, Anderson SJ, Bergh J, Dodwell D, Ewertz M, Gray R, Jagsi R, Pierce L, Pritchard KI, Swain S, Wang Z, Wang Y, Whelan T, Peto R, McGale P, Early Breast Cancer Trialists' Collaborative Group (2017) Estimating the Risks of Breast Cancer Radiotherapy: Evidence From Modern Radiation Doses to the Lungs and Heart and From Previous Randomized Trials. J Clin Oncol 35 (15):1641-1649. doi:10.1200/JCO.2016.72.0722
5. PASSOS collaboration Personalised assessment of late health risks after exposure to ionising radiation and guidance for radiation applications in medicine. https://passos.helmholtz-muenchen.de. Accessed 9 July 2018
6. Wollschläger D, Karle H, Stockinger M, Bartkowiak D, Buhrdel S, Merzenich H, Wiegel T, Blettner M, Schmidberger H (2016) Radiation dose distribution in functional heart regions from tangential breast cancer radiotherapy. Radiother Oncol 119 (1):65-70. doi:10.1016/j.radonc.2016.01.020
7. Merzenich H, Bartkowiak D, Schmidberger H, Schmidt M, Schwentner L, Wiegel T, Woeckel A, Wollschlager D, Blettner M (2017) 3D conformal radiotherapy is not associated with the long-term cardiac mortality in breast cancer patients: a retrospective cohort study in Germany (PASSOS-Heart Study). Breast Cancer Res Treat 161 (1):143-152. doi:10.1007/s10549-016-4042-2
8. Wollschläger D, Karle H, Stockinger M, Bartkowiak D, Buhrdel S, Merzenich H, Wiegel T, Schmidberger H, Blettner M (2017) Predicting Heart Dose in Breast Cancer Patients Who Received 3D Conformal Radiation Therapy. Health Phys 112 (1):1-10. doi:10.1097/HP.0000000000000577
9. Wollschläger D, Merzenich H, Schwentner L, Janni W, Wiegel T, Bartkowiak D, Wockel A, Schmidt M, Schmidberger H, Blettner M (2017) Self-reported long-term

cardiac morbidity in breast cancer patients: a retrospective cohort study in Germany (PASSOS Heart Study). Breast Cancer Res Treat 163 (3):595-604. doi:10.1007/s10549-017-4215-7
10. Donovan EM, James H, Bonora M, Yarnold JR, Evans PM (2012) Second cancer incidence risk estimates using BEIR VII models for standard and complex external beam radiotherapy for early breast cancer. Med Phys 39 (10):5814-5824. doi:10.1118/1.4748332
11. Joosten A, Matzinger O, Jeanneret-Sozzi W, Bochud F, Moeckli R (2013) Evaluation of organ-specific peripheral doses after 2-dimensional, 3-dimensional and hybrid intensity modulated radiation therapy for breast cancer based on Monte Carlo and convolution/superposition algorithms: Implications for secondary cancer risk assessment. Radiother Oncol 106 (1):33-41. doi:10.1016/j.radonc.2012.11.012
12. Lee B, Lee S, Sung J, Yoon M (2014) Radiotherapy-induced secondary cancer risk for breast cancer: 3D conformal therapy versus IMRT versus VMAT. J Radiol Prot 34 (2):325-331. doi:10.1088/0952-4746/34/2/325
13. Han EY, Paudel N, Sung J, Yoon M, Chung WK, Kim DW (2016) Estimation of the risk of secondary malignancy arising from whole-breast irradiation: comparison of five radiotherapy modalities, including TomoHDA. Oncotarget 7 (16):22960-22969. doi:10.18632/oncotarget.8392
14. Santos AMC, Marcu LG, Wong CM, Bezak E (2016) Risk estimation of second primary cancers after breast radiotherapy. Acta Oncol 55 (11):1331-1337. doi:10.1080/0284186x.2016.1185150
15. Joosten A, Bochud F, Moeckli R (2014) A critical evaluation of secondary cancer risk models applied to Monte Carlo dose distributions of 2-dimensional, 3-dimensional conformal and hybrid intensity-modulated radiation therapy for breast cancer. Phys Med Biol 59 (16):4697-4722. doi:10.1088/0031-9155/59/16/4697
16. NCD Risk Factor Collaboration (2016) A century of trends in adult human height. eLife 5:e13410. doi:10.7554/eLife.13410
17. Fippel M (1999) Fast Monte Carlo dose calculation for photon beams based on the VMC electron algorithm. Med Phys 26 (8):1466-1475. doi:10.1118/1.598676
18. Fippel M, Haryanto F, Dohm O, Nusslin F, Kriesen S (2003) A virtual photon energy fluence model for Monte Carlo dose calculation. Med Phys 30 (3):301-311. doi:10.1118/1.1543152
19. Kriesen S, Fippel M (2005) [Verification of the VEF photon beam model for dose calculations by the Voxel-Monte-Carlo-Algorithm]. Z Med Phys 15 (2):115-121
20. Grantzau T, Thomsen MS, Vaeth M, Overgaard J (2014) Risk of second primary lung cancer in women after radiotherapy for breast cancer. Radiother Oncol 111 (3):366-373. doi:10.1016/j.radonc.2014.05.004
21. Stovall M, Smith SA, Langholz BM, Boice JD, Jr., Shore RE, Andersson M, Buchholz TA, Capanu M, Bernstein L, Lynch CF, Malone KE, Anton-Culver H, Haile RW, Rosenstein BS, Reiner AS, Thomas DC, Bernstein JL, Women's Environmental Cancer and Radiation Epidemiology Study Collaborative Group (2008) Dose to the contralateral breast from radiotherapy and risk of second primary breast cancer in the WECARE study. Int J Radiat Oncol Biol Phys 72 (4):1021-1030. doi:10.1016/j.ijrobp.2008.02.040
22. Morton LM, Gilbert ES, Hall P, Andersson M, Joensuu H, Vaalavirta L, Dores GM, Stovall M, Holowaty EJ, Lynch CF, Curtis RE, Smith SA, Kleinerman RA, Kaijser M, Storm HH, Pukkala E, Weathers RE, Linet MS, Rajaraman P, Fraumeni JF, Jr., Brown LM, van Leeuwen FE, Fossa SD, Johannesen TB, Langmark F, Lamart S, Travis LB,

Aleman BM (2012) Risk of treatment-related esophageal cancer among breast cancer survivors. Ann Oncol 23 (12):3081-3091. doi:10.1093/annonc/mds144
23. Preston DL, Ron E, Tokuoka S, Funamoto S, Nishi N, Soda M, Mabuchi K, Kodama K (2007) Solid cancer incidence in atomic bomb survivors: 1958-1998. Radiat Res 168 (1):1-64. doi:10.1667/RR0763.1
24. Zentrum für Krebsregisterdaten (2014) Robert Koch-Institut. http://www.krebsdaten.de/Krebs/DE/Datenbankabfrage/datenbankabfrage_stufe1_node.html. Accessed 26 March 2017
25. Ferlay J, Steliarova-Foucher E, Lortet-Tieulent J, Rosso S, Coebergh JW, Comber H, Forman D, Bray F (2013) Cancer incidence and mortality patterns in Europe: estimates for 40 countries in 2012. Eur J Cancer 49 (6):1374-1403. doi:10.1016/j.ejca.2012.12.027
26. Blettner M, Boice JD, Jr. (1991) Radiation dose and leukaemia risk: general relative risk techniques for dose-response models in a matched case-control study. Stat Med 10 (10):1511-1526
27. Curtis RE, Boice JD, Jr., Stovall M, Bernstein L, Holowaty E, Karjalainen S, Langmark F, Nasca PC, Schwartz AG, Schymura MJ, et al. (1994) Relationship of leukemia risk to radiation dose following cancer of the uterine corpus. J Natl Cancer Inst 86 (17):1315-1324
28. Cristy M (1981) Active bone marrow distribution as a function of age in humans. Phys Med Biol 26 (3):389-400
29. Schneider U, Zwahlen D, Ross D, Kaser-Hotz B (2005) Estimation of radiation-induced cancer from three-dimensional dose distributions: Concept of organ equivalent dose. Int J Radiat Oncol Biol Phys 61 (5):1510-1515. doi:10.1016/j.ijrobp.2004.12.040
30. Aznar MC, Duane FK, Darby SC, Wang Z, Taylor CW (2018) Exposure of the lungs in breast cancer radiotherapy: A systematic review of lung doses published 2010-2015. Radiother Oncol 126 (1):148-154. doi:10.1016/j.radonc.2017.11.022
31. Joosten A, Bochud F, Baechler S, Levi F, Mirimanoff RO, Moeckli R (2011) Variability of a peripheral dose among various linac geometries for second cancer risk assessment. Phys Med Biol 56 (16):5131-5151. doi:10.1088/0031-9155/56/16/004
32. Berrington de Gonzalez A, Gilbert E, Curtis R, Inskip P, Kleinerman R, Morton L, Rajaraman P, Little MP (2013) Second solid cancers after radiation therapy: a systematic review of the epidemiologic studies of the radiation dose-response relationship. Int J Radiat Oncol Biol Phys 86 (2):224-233. doi:10.1016/j.ijrobp.2012.09.001
33. Trott KR (2009) Second cancers after radiotherapy. In: Joiner MC, van der Kogel A (eds) Basic Clinical Radiobiology. 4 edn. CRC Press,
34. Sachs RK, Brenner DJ (2005) Solid tumor risks after high doses of ionizing radiation. Proc Natl Acad Sci USA 102 (37):13040-13045. doi:10.1073/pnas.0506648102
35. Schneider U, Kaser-Hotz B (2005) Radiation risk estimates after radiotherapy: application of the organ equivalent dose concept to plateau dose-response relationships. Radiat Environ Biophys 44 (3):235-239. doi:10.1007/s00411-005-0016-1
36. National Council on Radiation Protection and Measurements (2011) Second Primary Cancers and Cardiovascular Disease After Radiation Therapy.
37. Corradini S, Ballhausen H, Weingandt H, Freislederer P, Schonecker S, Niyazi M, Simonetto C, Eidemüller M, Ganswindt U, Belka C (2018) Left-sided breast cancer and risks of secondary lung cancer and ischemic heart disease : Effects of modern

radiotherapy techniques. Strahlenther Onkol 194 (3):196-205. doi:10.1007/s00066-017-1213-y
38. Berrington de Gonzalez A, Curtis RE, Gilbert E, Berg CD, Smith SA, Stovall M, Ron E (2010) Second solid cancers after radiotherapy for breast cancer in SEER cancer registries. Br J Cancer 102 (1):220-226. doi:10.1038/sj.bjc.6605435
39. Rusner C, Wolf K, Bandemer-Greulich U, Engel J, Stegmaier C, Holleczek B, Schubert-Fritschle G, Tillack A, Stang A (2014) Risk of contralateral second primary breast cancer according to hormone receptor status in Germany. Breast Cancer Res 16 (5). doi:10.1186/s13058-014-0452-4
40. Cuzick J, Sestak I, Pinder SE, Ellis IO, Forsyth S, Bundred NJ, Forbes JF, Bishop H, Fentiman IS, George WD (2011) Effect of tamoxifen and radiotherapy in women with locally excised ductal carcinoma in situ: long-term results from the UK/ANZ DCIS trial. Lancet Oncol 12 (1):21-29. doi:10.1016/S1470-2045(10)70266-7

Table 1 Overview of the different dosimetric approaches in this study. Risk estimates in this study are only based on the whole-body MC based calculations.

| | Planning System | Linear accelerator | Study group | Investigated techniques | Comments |
|---|---|---|---|---|---|
| Whole-body MC based calculations (see 'Organ dose assessment' in 'Methods') | IPLAN 4.5.4 | BrainLAB Vero | Single woman, both lateralities planned | 3D-CRT without wedges, Multi-field IMRT | Main approach; for validation see Figs. S4, S5, S6 |
| TLD measurements (see 'Different tangential techniques…' in 'Methods') | Oncentra Masterplan 4.3 | Siemens Primus | Alderson phantom | 3D-CRT without wedges, 3D-CRT with wedges, Hybrid IMRT | Used for Fig. 4 |
| Conventional treatment planning (see 'The PASSOS planning study' in the supplementary material) | Oncentra Masterplan 4.3 | Siemens Oncor | 50 BC patients | 3D-CRT without wedges, Multi-field IMRT | Used for Fig. S7 |
| | | Siemens Primus | 78 BC patients | 3D-CRT without wedges, 3D-CRT with wedges, Hybrid IMRT | Used for Fig. 4 |

Table 2 Estimated and observed relative risks for second primary cancers after breast cancer radiotherapy.

| | Lungs | Contralat. Breast | Oesophagus | Leukaemia (LNT) | Leukaemia (lin-exp) | Thyroid | Other |
|---|---|---|---|---|---|---|---|
| 3D-CRT | 1.37 (1.17; 1.91) | 1.11 (0.92; 1.30) | 1.05 (1.03; 1.09) | 1.12 (1.05; 1.23) | 1.2 (1.0; 2.1) | 1.11 (1.02; 1.32) | 1.04 (1.03; 1.06) |
| IMRT | 1.48 (1.23; 2.19) | 1.56 (0.62; 2.49) | 1.10 (1.06; 1.17) | 1.20 (1.08; 1.37) | 1.4 (0.9; 2.9) | 1.16 (1.03; 1.45) | 1.07 (1.05; 1.11) |
| Clarke et al. | 1.61 (1.31; 1.91) | 1.18 (1.08; 1.28) | 2.06 (1.19; 2.93) | 1.71 (1.12; 2.30) | | 0.69 (0.13; 1.25) | 1.08 (0.96; 1.20) |

The first two rows show relative risks compared to an unexposed person, estimated in the present study from doses derived by Monte Carlo planning, for 3D-CRT without wedges and multi-field IMRT. The 90% confidence intervals were derived from the 90% or, by scaling, 95% confidence intervals of the risk coefficients and do not take into account other sources of uncertainty. The last row is adopted from ref. [3] and shows the relative risks and 90% confidence intervals (scaled from standard errors) comparing women treated for breast cancer with and without radiotherapy.

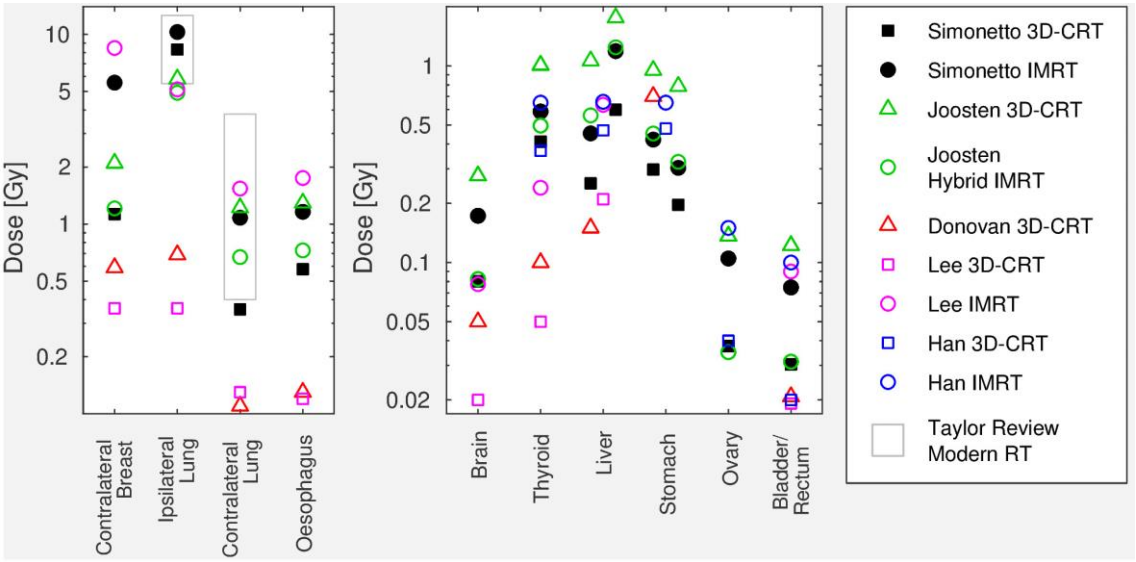


**Fig. 1** Mean organ doses as determined by Monte Carlo planning or measurements in a phantom, as taken from this study (solid, black symbols) and refs. [10-13]. For comparison, the interquartile range of mean lung doses in modern radiotherapy is shown as determined by a review of the literature [4]. While circles are used to denote IMRT techniques, squares are reserved for 3D-CRT without physical wedges and triangles for wedged 3D-CRT. For the hybrid IMRT, Joosten et al. used the same main tangents as for the 3D-CRT technique plus two additional tangential fields. Han et al. present organ equivalent doses instead of mean doses and the dose to the rectum instead of the bladder. As different estimates are available for left- and right-sided radiotherapy in the publication of Joosten et al. and in the present manuscript, both estimates are plotted for liver and stomach with markers shifted slightly to the left and to the right, respectively. Only left-sided radiotherapy was evaluated by Donovan et al.; Han et al. present only the average of both lateralities, and no information on laterality is given by Lee et al. Overlying estimates were piled up. Note the logarithmic scale.

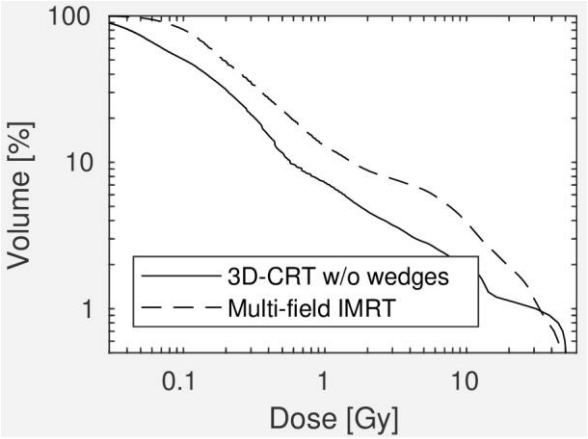


**Fig. 2** Dose-volume histogram of the active bone marrow as calculated by a Monte Carlo based treatment planning system in a whole-body CT.

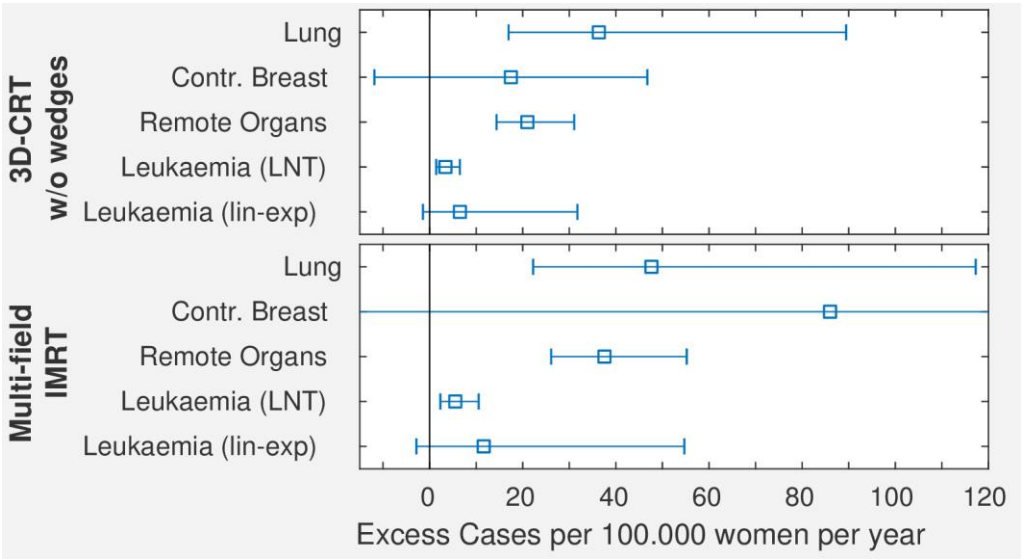


**Fig. 3** Estimated absolute risks as obtained by multiplication of relative risks and population incidence rates for women with an age of at least 50 years. Illustrated error bars refer to 90% confidence intervals of the underlying risk coefficients and do not include other sources of uncertainty.

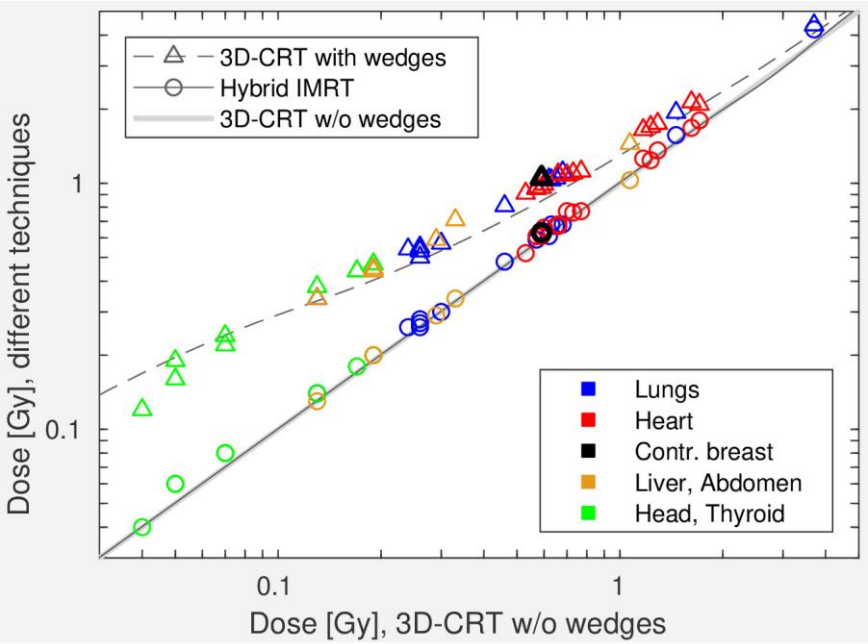


**Fig. 4** Comparison of doses from different tangential treatment techniques. Markers show the doses from 3D-CRT with wedges and from hybrid IMRT, measured in different positions in a phantom plotted against the dose measured at the same position when applying the 3D-CRT technique without wedges. In the online version, colours inform about the position within the phantom. Lines show the average calculated dose distribution in the PASSOS planning study plotted against the average planned dose distribution when applying the 3D-CRT technique without wedges. The identity is included as a grey line for reference.

**Supplementary Material:**

# Exposure of Remote Organs and Associated Cancer Risks from Tangential and Multi-Field Breast Cancer Radiotherapy

C. Simonetto*, H. Rennau, J. Remmele, S. Sebb, P. Kundrát, M. Eidemüller, U. Wolf, G. Hildebrandt

*cristoforo.simonetto@helmholtz-muenchen.de, Institute of Radiation Protection, Helmholtz Zentrum München Deutsches Forschungszentrum für Gesundheit und Umwelt (GmbH), Ingolstädter Landstraße 1, 85764 Neuherberg, Germany

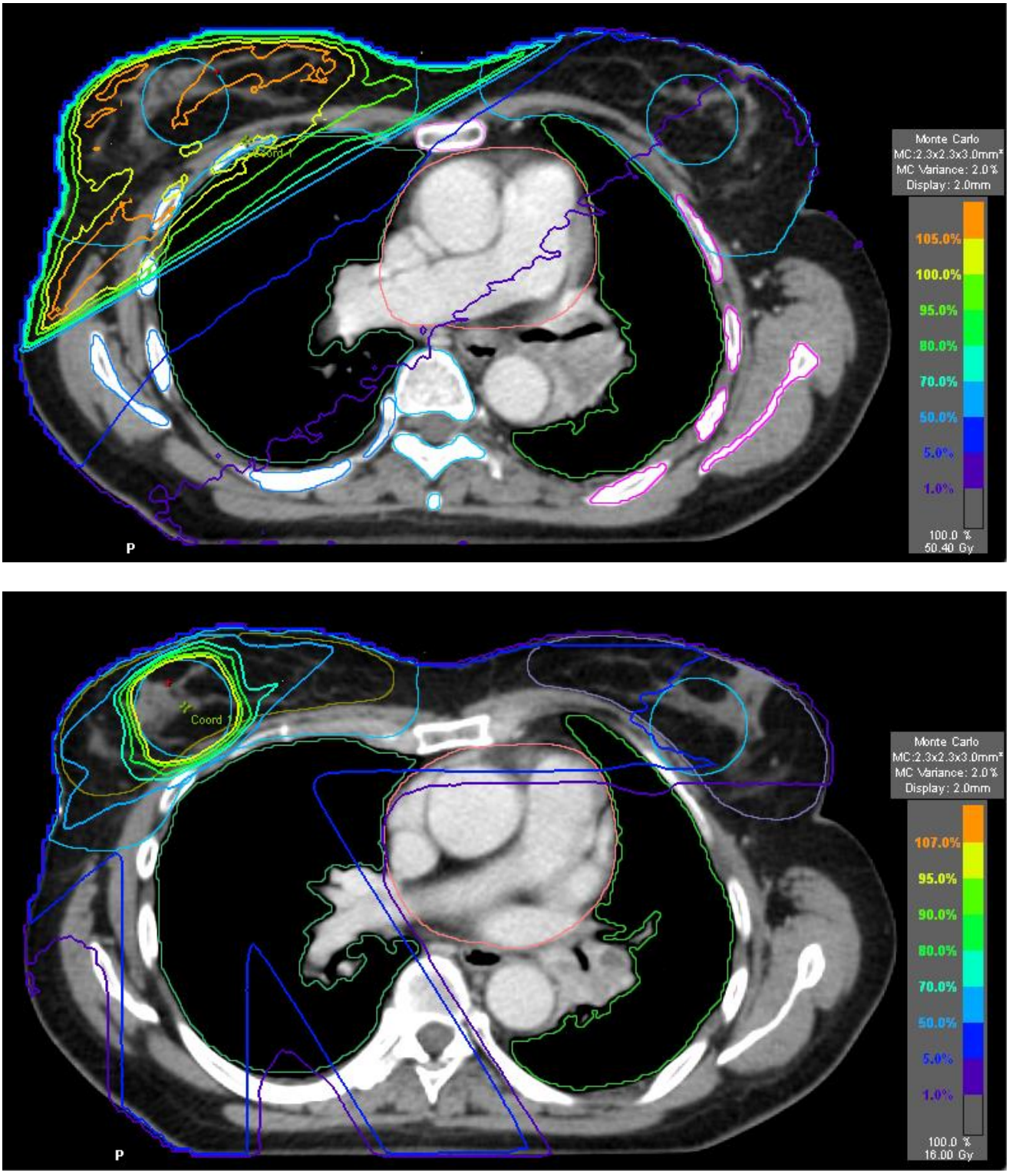


Figure S1. Dose distribution for 3D-CRT calculated with the Voxel-Monte-Carlo method (IPLAN) for PTV (upper panel, 100% correspond to 50.4 Gy) and boost volume (lower panel, 100% correspond to 16 Gy) within the whole-body CT.

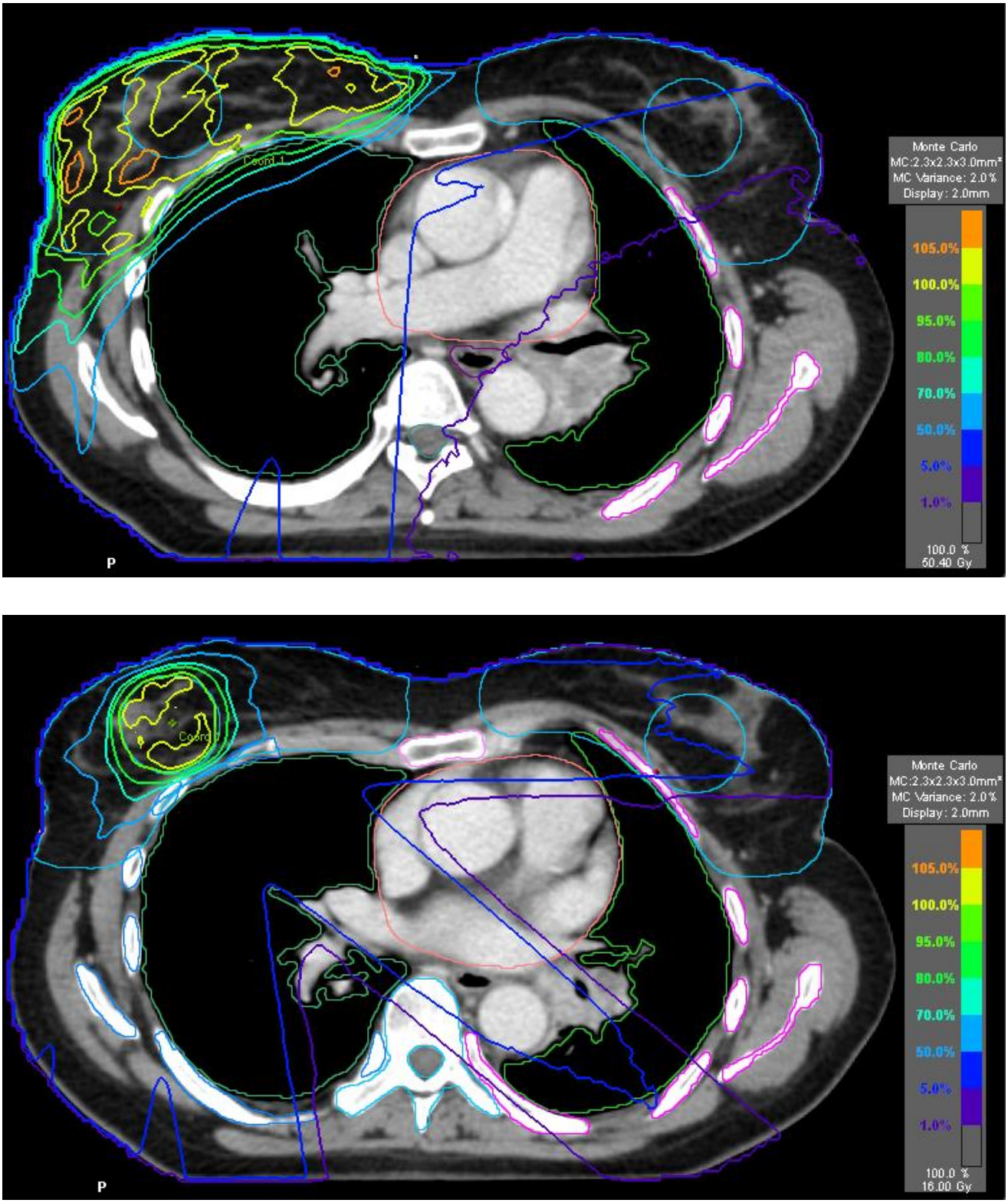


Figure S2. Dose distribution for multi-field IMRT calculated with the Voxel-Monte-Carlo method (IPLAN) for PTV (upper panel, 100% correspond to 50.4 Gy) and boost volume (lower panel, 100% correspond to 16 Gy) within the whole-body CT.

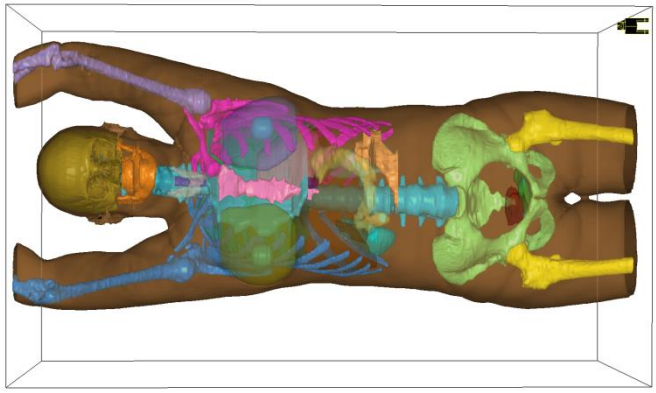

Figure S3: Whole-body female CT data used for treatment planning in the present manuscript with several organs being contoured.

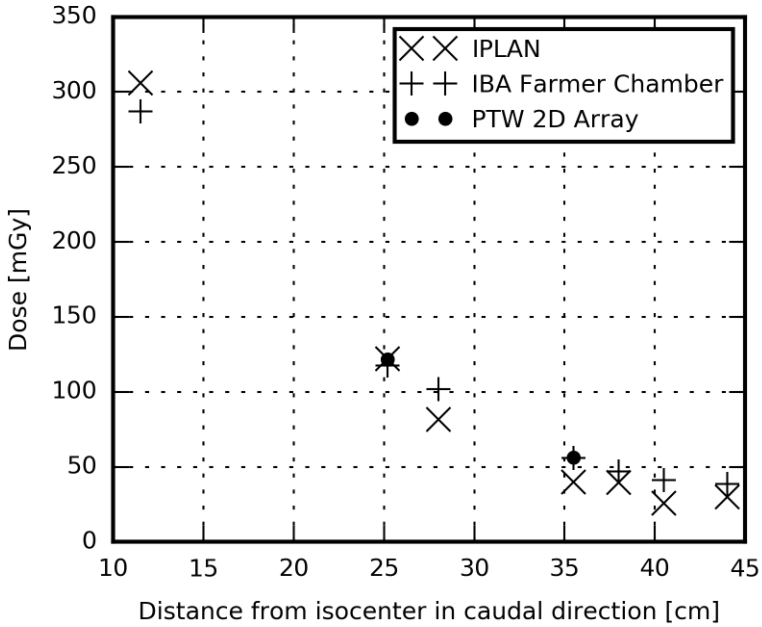


Figure S4. Calculated and measured dose profile in an anthropomorphic Alderson-Rando phantom in caudal direction. The area between left and right breast was irradiated with a 10x10 cm² open field (Vero, 4500 monitor units, 6 MV, source-to-surface distance of 100 cm). Doses were assessed 15 cm above table surface. Dose calculations with IPLAN 4.5.4 were averaged over a radius of 5 mm (dose matrix: 1x1mm in lateral direction and a CT slice thickness of 3mm). The measurements were performed with Farmer Chambers (IBA FC23-C) and a 2D Array (PTW OCTAVIUS 729).

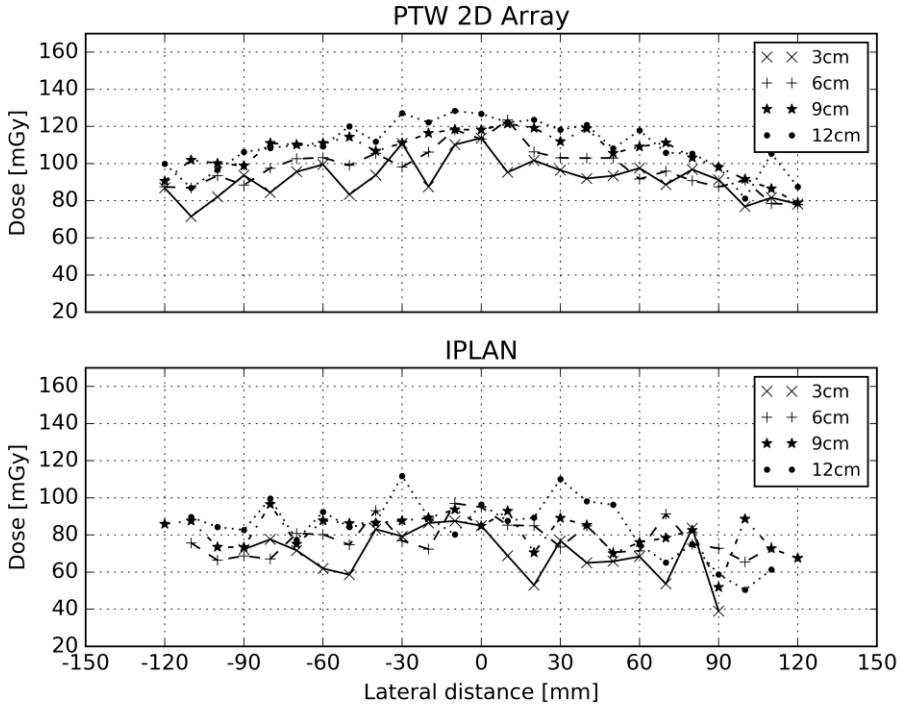


Figure S5. Lateral dose profiles at 25.2 cm caudal distance from the isocenter of the applied 10x10 field comparing ionisation chamber measurements (upper panel) against the dose calculation from the treatment planning system (lower panel). Dose profiles were taken at four different distances from the table surface: 3, 6, 9, 12 cm. The same setup was applied as for Figure S4.

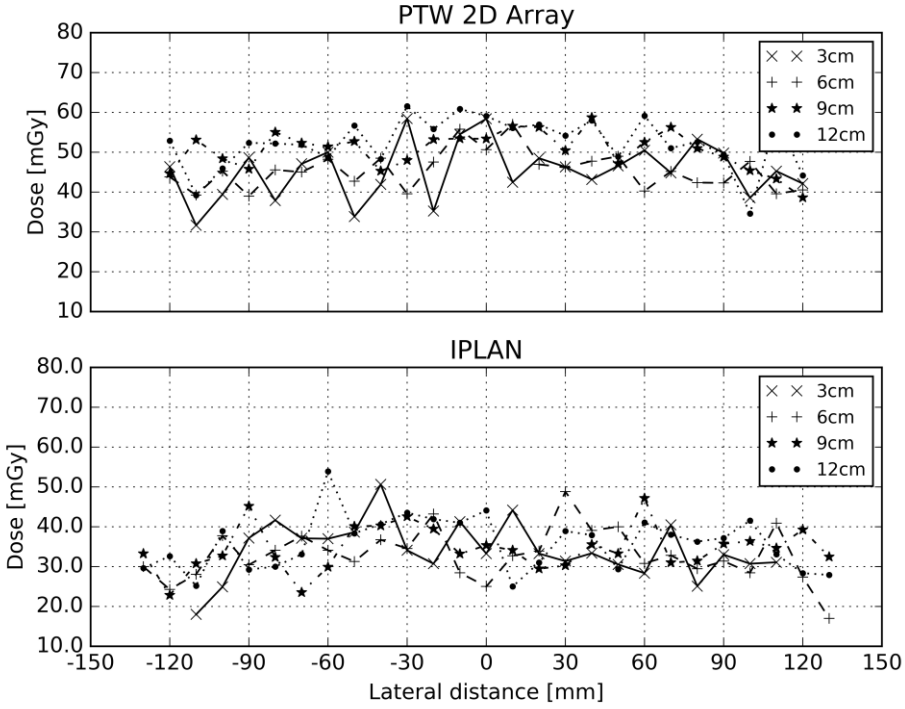


Figure S6. Lateral dose profiles at 35.5 cm caudal distance from the isocenter of the applied 10x10 field comparing ionisation chamber measurements (upper panel) against the dose calculation from the treatment planning system (lower panel). The same setup was applied as for Figure S5.

Table S1. Dose surrogate organs and incidence rates according to different endpoints as specified by ICD-10 codes.

| ICD-10 codes | Short description | Dose surrogate organ | Inc. rate |
|---|---|---|---|
| C00-C10, C12-C14 | Lip, oral cavity, pharynx | Mandible | 17.6 |
| C11, C30, C31, C69 | Nasopharynx, nasal cavity, eye | Brain | 3.6 |
| C15 | Oesophagus | Oesophagus | 8.0 |
| C16 | Stomach | Stomach | 30.7 |
| C17 | Small Intestine | Vertebrae (lowest 25%) | 5.0 |
| C18 | Colon | 0.33 Stomach (lowest 25%)<br>0.67 Vertebrae (lowest 25%) | 95.5 |
| C19-C21 | Rectosigmoid, rectum, anus | Bladder | 45.6 |
| C22 | Liver | Liver | 13.8 |
| C23, C24 | Gallbladder | Stomach (lowest 75%, other laterality) | 15.7 |
| C25 | Pancreas | Stomach (lowest 75%, same laterality) | 44.7 |
| C26 | Spleen, other and ill-defined digestive organs | 0.33 Stomach<br>0.67 Vertebrae | 2.6 |
| C32 | Larynx | Thyroid | 2.6 |
| C33, C34 | Trachea, lung | Lungs | 98.5 |
| C37 | Thymus | Heart (lowest 50%) | 0.5 |
| C38 | Heart | Heart | 0.5 |
| C39 | Other and ill-defined sites in respiratory system | Lungs | 0.0 |
| C50 | Breast | Contralateral breast | 309 |
| C51, C52, C68 | Vulva, vagina, other urinary organs | Bladder | 18.4 |
| C53-C55 | Uterus | Uterus | 68.5 |
| C56 | Ovary | Ovaries | 34.4 |
| C57 | Other female genital organs | Uterus | 3.7 |
| C58 | Placenta | Uterus | 0.0 |
| C64 | Kidney | Kidneys | 27.3 |
| C65, C66 | Renal pelvis, ureter | Kidneys | 4.4 |
| C67 | Bladder | Bladder | 21.8 |
| C70, C71 | Meninges, brain | Brain | 13.2 |
| C72 | Spinal cord, cranial nerves | Spinal cord | 0.2 |
| C73 | Thyroid gland | Thyroid | 12.4 |
| C74 | Adrenal gland | Kidneys | 0.6 |
| C75 | Other endocrine glands | 0.33 Brain<br>0.33 Thyroid<br>0.33 Spinal cord | 0.4 |
| C91-C95 | Leukaemia | Bone Marrow | 28.3 |

For some endpoints, only parts of the dose-volume histograms of adjacent organs were applied, for example the dose to the less exposed half of the heart served as a surrogate for the mean dose to the thymus. Average dose of a few adjacent organs was applied for ICD-10 codes C18, C26 and C75 as outlined in the table and, additionally, to derive the bone marrow dose as explained in the main text. This averaging resulted for example for the colon in 0.1 Gy for 3D-

CRT without wedges and 0.18 Gy for multi-field IMRT. Incidence rates were provided by the Robert Koch-Institut at www.krebsdaten.de and are presented as the number of cases in 100.000 women with an age above 50 years in Germany in the year 2014.

Table S2. Studies of second cancer after radiotherapy and coefficients used for linear risk estimates in some organs in relative vicinity to the treated breast together with 95% confidence intervals.

| Publication | Endpoints applied to | $ERR_{pd}$ [$Gy^{-1}$] |
|---|---|---|
| Grantzau, Thomsen, Vaeth, et al. Radiother Oncol. 2014; 111(3):366 | Lung (C33, C34) | 0.085 (0.031; 0.233) |
| Stovall, Smith, Langholu, et al. Int J Radiat Oncol Biol Phys. 2008; 72(4):1021 | Breast (C50) | 0.1 (-0.1; 0.3) |
| Morton, Gilber, Hall, et al. Ann Oncol. 2012; 23(12):3081 | Oesophagus (C15) | 0.09 (0.04; 0.16) |
| Curtis, Boice, Stovall, et al. J Natl Cancer Inst. 1994; 86(17):1315 | Leukaemia (C91-C95) | 0.13 (0.04; 0.27) |

Table S3. Excess relative risks [$Gy^{-1}$] for remote organs together with 90% confidence intervals as derived from the atomic bomb survivors.

| | |
|---|---|
| Lip, oral cavity, pharynx (C00-C14) | 0.39 (0.11; 0.76) |
| Stomach (C16) | 0.25 (0.12; 0.44) |
| Colon (C18) | 0.55 (0.15; 1.2) |
| Rectum (C19-C21) | 0.19 (-0.04; 0.47) |
| Liver (C22) | 0.32 (0.07; 0.85) |
| Gallbladder (C23, C24) | -0.05 (< -0.3; 0.3) |
| Pancreas (C25) | 0.26 (< -0.07; 0.68) |
| Uterus (C53-C55) | 0.1 (-0.09; 0.33) |
| Ovary (C56) | 0.61 (0.0; 1.5) |
| Renal Cell (C64) | 0.13 (-0.25; 0.75) |
| Bladder (C67) | 1.15 (0.34; 2.5) |
| Central nervous system (C70-C72) | 0.62 (0.21; 1.2) |
| Thyroid (C73) | 0.27 (0.05; 0.77) |
| Other in (C00-C39, C50-C75) | 0.51 (0.14; 1.1) |

Values are taken from Table 11 in Preston, Ron, Tokuoka, et al., Radiat Res. 2007;168(1):1, for an age at exposure of 50 years and attained age of 70 years.

Table S4. Weights of different compartments of the bone marrow-containing skeleton.

| Head | Mandible | Ribs, clavicles, scapulae | Sternum | Vertebrae | Sacrum, os coxae | Humeri | Femora (proximal part) |
|---|---|---|---|---|---|---|---|
| 7.6% | 0.8% | 19.7% | 3.1% | 32.3% | 27.4% | 2.3% | 6.7% |

Weights are based on Cristy, Phys Med Biol. 1981;26(3):389 and resemble the relative fractions of active bone marrow.

Table S5. Mean absorbed doses [Gy] for several organs and compartments of the skeleton as calculated by the Monte Carlo algorithm using a whole-body CT of a single person.

| | | Brain | Thyroid | Contr. Breast | Lungs | Heart (L) | Heart (R) | Oesophagus | Spinal cord | Liver (L) | Liver (R) | Stomach (L) | Stomach (R) | Kidneys | Ovaries | Uterus | Bladder |
|---|---|---|---|---|---|---|---|---|---|---|---|---|---|---|---|---|---|
| 3D-CRT without wedges | WBI | 0.07 | 0.39 | 0.73 | 3.9 | 4.5 | 0.64 | 0.43 | 0.20 | 0.23 | 0.57 | 0.27 | 0.18 | 0.17 | 0.03 | 0.03 | 0.02 |
| | WBI+ Boost | 0.08 | 0.41 | 1.1 | 4.3 | 4.9 | 0.75 | 0.58 | 0.31 | 0.25 | 0.60 | 0.30 | 0.20 | 0.19 | 0.01 | 0.04 | 0.03 |
| Multi- field IMRT | WBI | 0.16 | 0.56 | 5.2 | 5.3 | 5.2 | 1.4 | 0.85 | 0.39 | 0.43 | 1.2 | 0.39 | 0.28 | 0.31 | 0.09 | 0.07 | 0.07 |
| | WBI+ Boost | 0.17 | 0.59 | 5.6 | 5.7 | 5.8 | 1.7 | 1.2 | 0.46 | 0.45 | 1.2 | 0.42 | 0.30 | 0.34 | 0.10 | 0.08 | 0.07 |

| | | Head | Mandible | Ribs, clavicles, scapulae | Sternum | Vertebrae | Sacrum, os coxae | Humeri | Femora (prox.) | Bone Marrow |
|---|---|---|---|---|---|---|---|---|---|---|
| 3D-CRT without wedges | WBI | 0.07 | 0.19 | 3.3 | 3.2 | 0.19 | 0.04 | 0.27 | 0.02 | 0.84 |
| | WBI+ Boost | 0.08 | 0.21 | 3.6 | 3.8 | 0.27 | 0.04 | 0.28 | 0.02 | 0.93 |
| Multi- field IMRT | WBI | 0.15 | 0.31 | 5.0 | 7.8 | 0.45 | 0.09 | 0.31 | 0.05 | 1.4 |
| | WBI+ Boost | 0.17 | 0.34 | 5.2 | 8.3 | 0.51 | 0.11 | 0.33 | 0.06 | 1.5 |

If not otherwise specified, the mean of left- (L) and right- (R) sided treatment is shown. Uncertainty in the Monte Carlo calculations is about 30% for peripheral doses, see Figures S4-S6. Results in the main text refer to a treatment including whole-breast (WBI) and boost irradiation.

***The PASSOS planning study***

Aim of the PASSOS planning study was to compare organ dose distributions between different radiotherapy techniques for breast cancer treatment after breast conserving surgery. For 50 breast cancer patients both, a field-in-field 3D-CRT and a step-and-shoot multi-field IMRT plan were generated. As for the techniques studied in the main text, 6 MV photon beams were applied with flattening filters but no wedges, and the prescribed dose was 50.4 Gy to the whole breast plus an additional boost of 16 Gy to the tumour bed. The plans were generated with the same objectives and constraints, and by the same medical physicist as the Monte Carlo plans in the main text. However, treatment planning was performed on standard breast cancer CTs with Oncentra Masterplan 4.3, commissioned for the Siemens Oncor Impression Plus (Siemens AG, Healthcare, Erlangen, Germany), and the Collapsed Cone algorithm [20] was used for dose calculation. For two patients, the thyroid extended beyond the CT plan and corresponding doses could thus not be determined.

[Moreover, for 78 breast cancer patients different tangential plans were generated. The techniques were exactly identical to the ones studied with thermoluminescence detectors in a phantom in the main text.]

To illustrate individual variations in organ doses and to investigate the representativeness of the whole-body CT used for Monte Carlo calculations in the main text, an overview of the mean doses to the lungs, heart, contralateral breast, oesophagus, and thyroid is shown in Figure S7. Doses obtained from the whole-body CT are plotted as vertical red lines. Boxplots show the distribution of mean organ doses in the PASSOS planning study. For comparableness, all plans were calculated with the Collapsed Cone algorithm and planned as described above. Compared to 3D-CRT, larger inter-individual variation and typically higher mean doses were observed in multi-field IMRT plans. The whole-body CT doses lie outside the interquartile range of PASSOS study doses for the contralateral breast, and partially for the heart and oesophagus. For IMRT, mean dose to the contralateral breast in the whole-body CT was even about twice as large as for the median of the PASSOS study but nevertheless within normal variation. Finally, it needs to be stressed that in order to illustrate the inter-patient variability in Figure S7, the same, computationally efficient, treatment planning system (see above) was applied to all patient CTs. However, a Monte Carlo Based treatment planning system (see the Methods section) was used for Table S5 that was more accurate at low doses. Due to the different plans, results for the whole-body CT differ between Figure S7 and Table S5, and results of the main text are based on the latter.

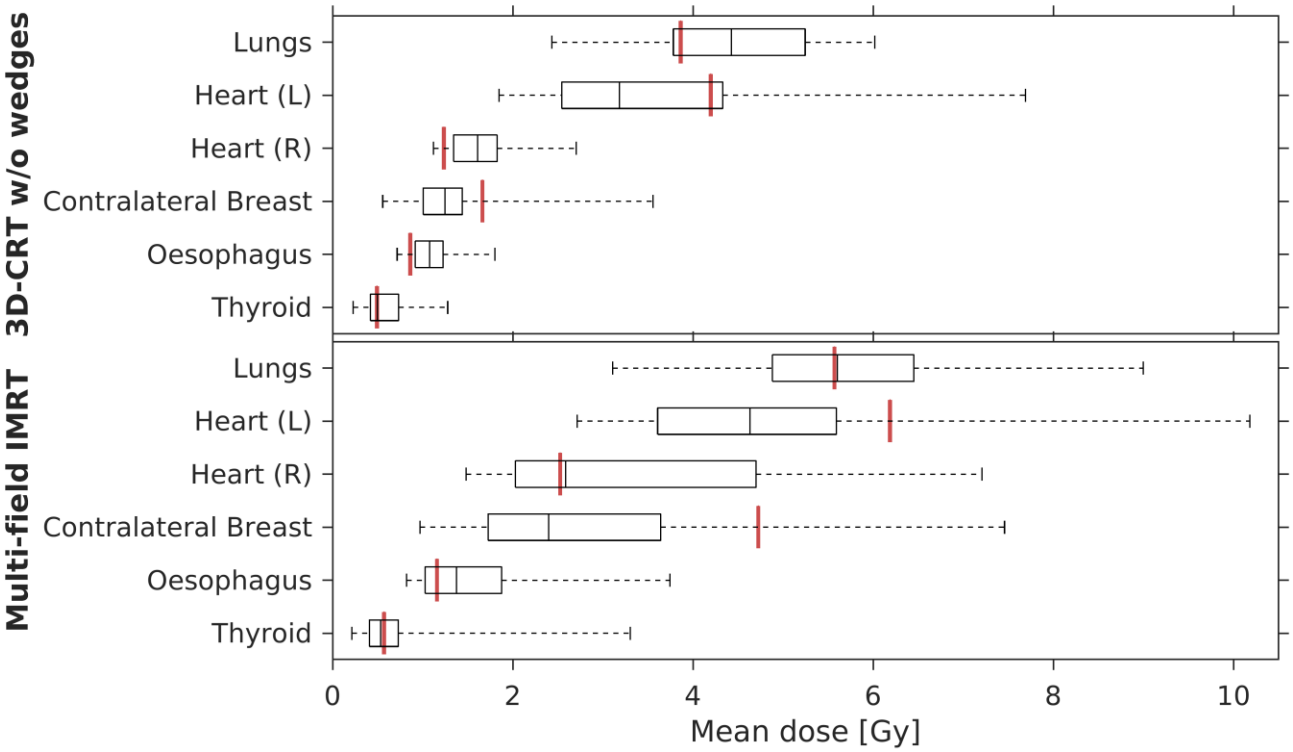


Figure S7. Boxplots showing the distribution of mean doses in several organs within 50 patients of the PASSOS planning study as calculated with the Collapsed Cone algorithm. Whiskers extend to the extreme values within the patient data set. The red lines correspond to the mean organ doses calculated for the single whole-body CT for which risk estimates are derived in the main text of the publication. L (R) refers to left- (right-) sided treatment.